

ARTICLE

Received 2 Oct 2013 | Accepted 29 Apr 2014 | Published 5 Jun 2014

DOI: 10.1038/ncomms4997

Hybrid multiphoton volumetric functional imaging of large-scale bioengineered neuronal networks

Hod Dana^{1,*†}, Anat Marom^{1,2,*}, Shir Paluch¹, Roman Dvorkin³, Inbar Brosh¹ & Shy Shoham¹

Planar neural networks and interfaces serve as versatile *in vitro* models of central nervous system physiology, but adaptations of related methods to three dimensions (3D) have met with limited success. Here, we demonstrate for the first time volumetric functional imaging in a bioengineered neural tissue growing in a transparent hydrogel with cortical cellular and synaptic densities, by introducing complementary new developments in nonlinear microscopy and neural tissue engineering. Our system uses a novel hybrid multiphoton microscope design combining a 3D scanning-line temporal-focusing subsystem and a conventional laser-scanning multiphoton microscope to provide functional and structural volumetric imaging capabilities: dense microscopic 3D sampling at tens of volumes per second of structures with mm-scale dimensions containing a network of over 1,000 developing cells with complex spontaneous activity patterns. These developments open new opportunities for large-scale neuronal interfacing and for applications of 3D engineered networks ranging from basic neuroscience to the screening of neuroactive substances.

¹Department of Biomedical Engineering, Technion—Israel Institute of Technology, Haifa 32000, Israel. ²The Interdepartmental Program in Biotechnology, Technion—Israel Institute of Technology, Haifa 32000, Israel. ³Faculty of Medicine and Network Biology Research Laboratories, Technion—Israel Institute of Technology, Haifa 32000, Israel. †Present address: HHMI Janelia Farm Research Campus, Ashburn, Virginia, 20147, USA. *These authors contributed equally to this work. Correspondence and requests for materials should be addressed to S.S. (email: sshoham@bm.technion.ac.il).

Spatiotemporal neuronal activity patterns are the fundamental representation of information within the nervous system. The complexity of real neural circuits and experimental challenges associated with *in situ* pharmacological manipulation and light scattering have motivated the development of simplified and accessible *in vitro* experimental systems such as neural cell and slice cultures where many aspects of natural neural dynamics are reproduced¹. Such cultures retain many morphological, pharmacological and electrical properties of *in vivo* cortical networks² and allow much more detailed observation and manipulation options than available for intact brains^{3,4}, usually through the use of planar multielectrode arrays (MEAs)⁵. These powerful combined abilities to observe and/or manipulate network-wide activity together with access to synaptic physiology, have already led to discoveries on universal characteristics of neural circuits that were later reaffirmed in an *in vivo* setting (for example, homeostatic rescaling⁶). Nevertheless, two-dimensional cultures capture only a limited facet of central nervous system connectivity and local microenvironments' biological and biophysical properties derived from cell-matrix interaction⁷, motivating the recent development of 3D models^{8–10}. The development of 3D cultures and the associated interface technology has not yet advanced to a stage where it allows the generation and detailed monitoring of realistic central nervous system-like network models, with major challenges remaining on both fronts.

Although early attempts at extending MEA technology to 3D were demonstrated^{11,12}, it is generally accepted that optophysiology methods are optimally suited for the required non-contact, volumetric interfacing. Indeed, two-photon laser scanning microscopy (TPLSM) neuronal imaging using calcium-sensitive dyes or genetically-encoded indicators¹³ is routinely used to image the activity of small neuron ensembles *in vivo*. However, scanning methods cannot generally achieve dense 3D imaging—with the exception of technically advanced multiplexing schemes¹⁴, most systems developed for rapid TPLSM imaging were generally based on sparse sampling of space^{15–17} (which is movement sensitive), whereas dense volumetric image acquisition at rates of 10 Hz or more, as required for action potential detection¹⁸, is still generally considered a major challenge.

We developed a scanning-line temporal-focusing (SLITE) microscope for rapid volumetric multiphoton fluorescence imaging of a large field of view and here we show dense microscopic imaging of a novel 3D spontaneously active network with brain-approximating characteristics grown *in vitro* in an extracellular matrix-like hydrogel. In temporal focusing (TF) nonlinear microscopy, the laser pulse's duration, rather than its spatial dimensions, is manipulated ('focused') to generate optically-sectioned illumination of thin planes^{19–21}, lines^{22–24} or flexible patterns^{25–27} inside a 3D volume without the need for tight spatial focusing. Line illumination geometry, also referred to as simultaneous spatial and TF²³, was demonstrated to be suitable for rapid imaging²² and to have excellent sectioning capabilities inside a scattering medium²⁸. To effectively excite a long line simultaneously, our SLITE microscope uses a regeneratively amplified ultrafast laser source (RegA 9000, Coherent) which provides $\tau_a = 200$ fs pulses at $f_a = 150$ kHz repetition rate and an average power of 600 mW (4 μ J per pulse). Compared with standard Ti:Sapphire lasers, which are commonly used for TPLSM, and provide $\tau_s = 100$ fs pulses at $f_s = 80$ MHz repetition rate (7.5 nJ per pulse), the amplified laser enhances two-photon absorption by a factor of $\frac{\tau_{sf}}{\tau_{af}} = 266$ for identical average power. Moreover, since laser power remains a limiting factor for parallelized multiphoton excitation techniques even when an amplified laser source is used, our setup is based on a new

light-efficient design that also introduces the new ability to seamlessly switch between SLITE and TPLSM scanning modes; having this bi-modal imaging capability in the same sample turns out to provide crucial synergistic benefits for practical tissue imaging. Considering the unique constraints and requirements imposed by the dynamic structure of developing bioengineered tissue cultures, SLITE microscopy appears to be a particularly suitable imaging approach for monitoring their activity: unlike other state-of-the-art multiphoton imaging systems^{15–17}, our system creates structured, dense 3D stacks rather than rapid serial point-scans that require planning, optimizing and readjusting of sparse cell-crossing complex scan trajectories. Its excellent performance in lightly-scattering bioengineered tissue is limited primarily by the detection camera performance and imaging speed limits—200 frames per second in our experiments, and potentially orders-of-magnitude faster in future implementations.

Results

Rapid 3D SLITE-multiphoton microscope design. The dual-mode SLITE-multiphoton microscope schematic and method of operation are shown in Fig. 1. It is based on a new design concept for TF microscopy: whereas previous systems^{19–27} used reflective gratings where the light propagation direction is changed after being diffracted, light propagation in this system is along a single linear axis (Supplementary Note 1). This design is based on the use of a custom transmission diffraction grating, mounted between two prisms (dual-prism grating, DPG) and has three fundamental advantages. First, it enables a simple, seamless switch between TF and TPLSM, which were integrated here into a single system for the first time. Switching to SLITE mode simply requires introducing a DPG + cylindrical lens module instead of the scan lens, and rotating a dichroic mirror that deflects the emitted fluorescence signal towards an EMCCD camera (Fig. 1a). Second, since the imaging system is limited by pulse energy, the DPG's enhanced diffraction efficiency (85% in our setup) relative to reflective diffraction gratings (typically 50–70%), provides a major improvement in system characteristics (see also Supplementary Fig. 1). Third, DPG-based TF setup enables to remotely scan the focal plane²⁹, which may be useful in future applications. Plane imaging is achieved by lateral scanning of the illuminated line by operating one of the microscope's galvanometric mirrors (Fig. 1d, *xy* plane and Supplementary Movie 1); axial scanning is achieved by moving the objective lens using a piezoelectric device (Fig. 1d, *yz* plane and Supplementary Movie 1). When a large field-of-view objective lens is used ($\times 10$, NA = 0.45, Zeiss), the fundamental axial sectioning in our system is 13 μ m FWHM (Fig. 1b, consistent with a recent model²⁸). The dynamic elements of the system—scanning mirror, camera, piezoelectric device and a Pockels cell that attenuates the laser beam intensity, are synchronized to perform dense volumetric imaging (Supplementary Fig. 2).

Tissue-engineered 3D neuronal 'optonets'. Optimized protocols were developed for generating and maintaining the long-term growth and physiological viability of high-density bioengineered 3D networks of embryonic dissociated rat cortical cells inside an optically-accessible scaffold (Supplementary Fig. 3). Dissociated cell populations containing both neurons and glia encapsulated at high densities of 40,000–60,000 cells μ l⁻¹ in Matrigel extracellular matrix-like hydrogel scaffold, were maintained for 5–42 days in a medium containing a custom cocktail of growth supplements and neurotrophic growth factors that supported network development (Supplementary Movie 2). To characterize the networks' components and their viability, we applied a series of specialized stains which were imaged using a confocal

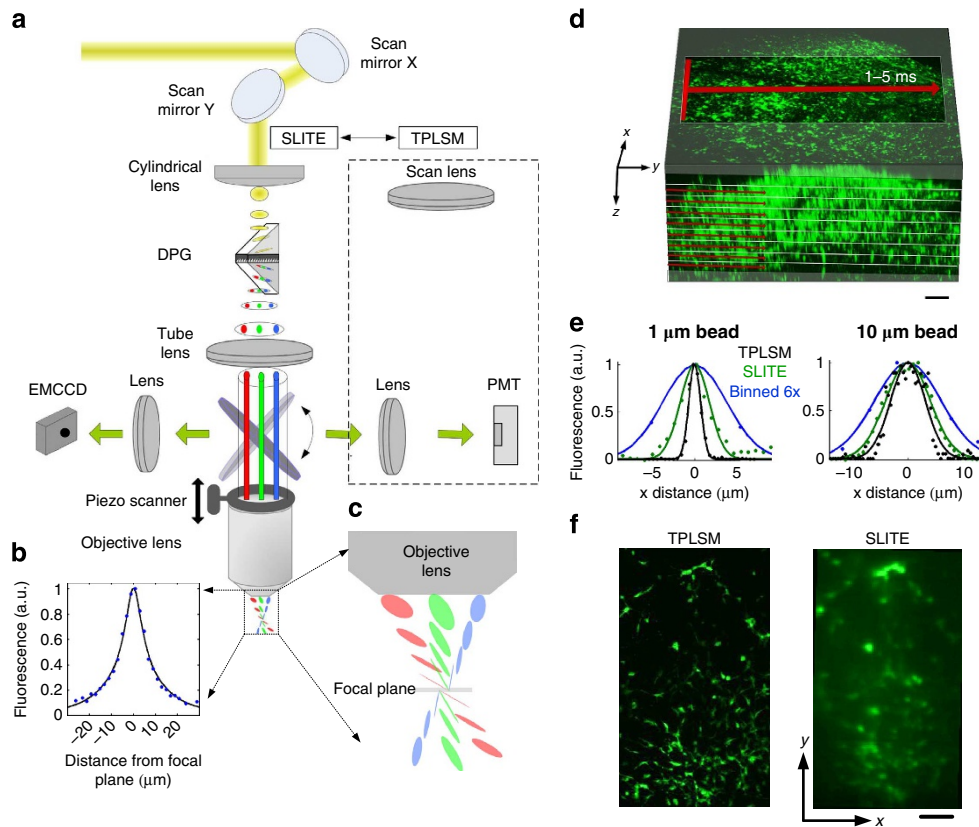


Figure 1 | Dual-mode TPLSM-SLITE microscope. (a) Optical scheme: in the single-axis SLITE mode a transmission grating diffracts the laser beam, but the central wavelength (800 nm) maintains its propagation direction due to refraction by the prism facets. For TPLSM, a scan lens replaces the cylindrical lens and DPG and the dichroic mirror redirects the fluorescence toward a photomultiplier tube (dashed line). (b) SLITE axial sectioning, measured values (dots) versus predicted²⁸ (line). (c) Expanded view of light propagation in focal volume. (d) A 3D imaging geometry: rapid functional SLITE imaging is performed in the volume first acquired using ‘structural’ TPLSM. A temporally focused *x* axis illuminated line is rapidly scanned in the *y* axis, while the objective is scanned axially. (e) Measured optical profiles of 1 μm (left) and 10 μm (\sim cell-sized, right) fluorescent beads, using TPLSM (black dots), SLITE (green dots) and SLITE with 6 \times 6 camera pixel binning (blue dots). Solid lines are Gaussian fits. (f) Z-projections of volumes acquired by TPLSM (0.5 Hz acquisition rate) and SLITE (200 Hz acquisition rate). Scale bar, 100 μm .

microscope. Using whole-gel differential immunostaining for glia (S100) and neurons (β III-tubulin), we established that both cell types are growing in the network (Fig. 2a and Supplementary Movie 3), with a stable 1:4 neuron:glia ratio reached by day 21 (Fig. 2b and Supplementary Fig. 4), indicating a fundamental similarity to normal cortical tissue. Both cellular subpopulations demonstrate a very high degree of cellular viability ($>95\%$ following network stabilization at day 14, Fig. 2c,d, Supplementary Fig. 5 and Supplementary Movie 4), which was found to be critically dependent on glial cell proliferation. Short treatment with the antiproliferative agent arabinofuranosyl cytidine (ARA-C) led to collective network degeneration which began during the second week of culturing (Fig. 2b,d,f, red lines; Supplementary Fig. 6). To study the characteristics of synaptic connectivity, fluorescently labelled synaptic proteins (Cerulean tagged SV2 and EGFP tagged PSD95) were time-lapse imaged over several days (Fig. 2c and Supplementary Movie 5). Neurons in the network develop a multitude of synaptic connections that in mature networks have spine densities ($0.5 \pm 0.1 \mu\text{m}^{-1}$; three experiments, DIV16–31, $n = 7$ neurons, 2,972 spines) comparable with these reported *in vivo* at similar developmental stages ($0.3\text{--}0.6 \mu\text{m}^{-1}$)³⁰. Younger preparations (DIV14–18) showed extensive growth and synaptogenesis, with a multitude of elongating axons and dendrites that freely invaded the embedding Matrigel, led by motile growth cones, and formed complex networks and new synapses. Older (DIV23–35) cultures

exhibited milder yet apparent growth dynamics and more stable synaptic connections. Cell growth and network evolution change the scattering characteristics of the sample, which gradually became more turbid, remaining far less scattering than cortical tissue³¹ (Supplementary Fig. 7). Networks generated spatiotemporally complex spontaneous activity patterns (Supplementary Movie 6) as early as DIV 5, whose activity rate and patterns also varied systematically with network age (Supplementary Fig. 8).

Rapid volumetric functional imaging. To volumetrically image spontaneous network physiology, we used the combined structural-functional TPLSM-SLITE approach to image networks that were bath-loaded with the fluorescent calcium indicator Fluo-4-AM ($n = 14$, DIV6–32). An imaging experiment began by acquiring TPLSM structural images of the tissue (as in Fig. 1d) followed by the acquisition of 10,000–150,000 3D-image SLITE movies of the same volume. Individual experiments used either a Zeiss $\times 10$ NA = 0.45 objective (FOV: $600 \times 1000 \mu\text{m}^2$, $n = 7$ networks with 922 ± 176 cells in FOV), or an Olympus $\times 20$ NA = 0.5 objective where the *xy* field of view is roughly halved (FOV: $250 \times 500 \mu\text{m}^2$, $n = 7$ networks with 201 ± 83 cells in FOV), while resolution is doubled. As the imaging rate bottleneck was EMCCD acquisition rate, we reduced the spatial resolution to 6 μm per pixel by binning adjacent pixels: binning reduced the SLITE spatial resolution but left cell-sized details roughly

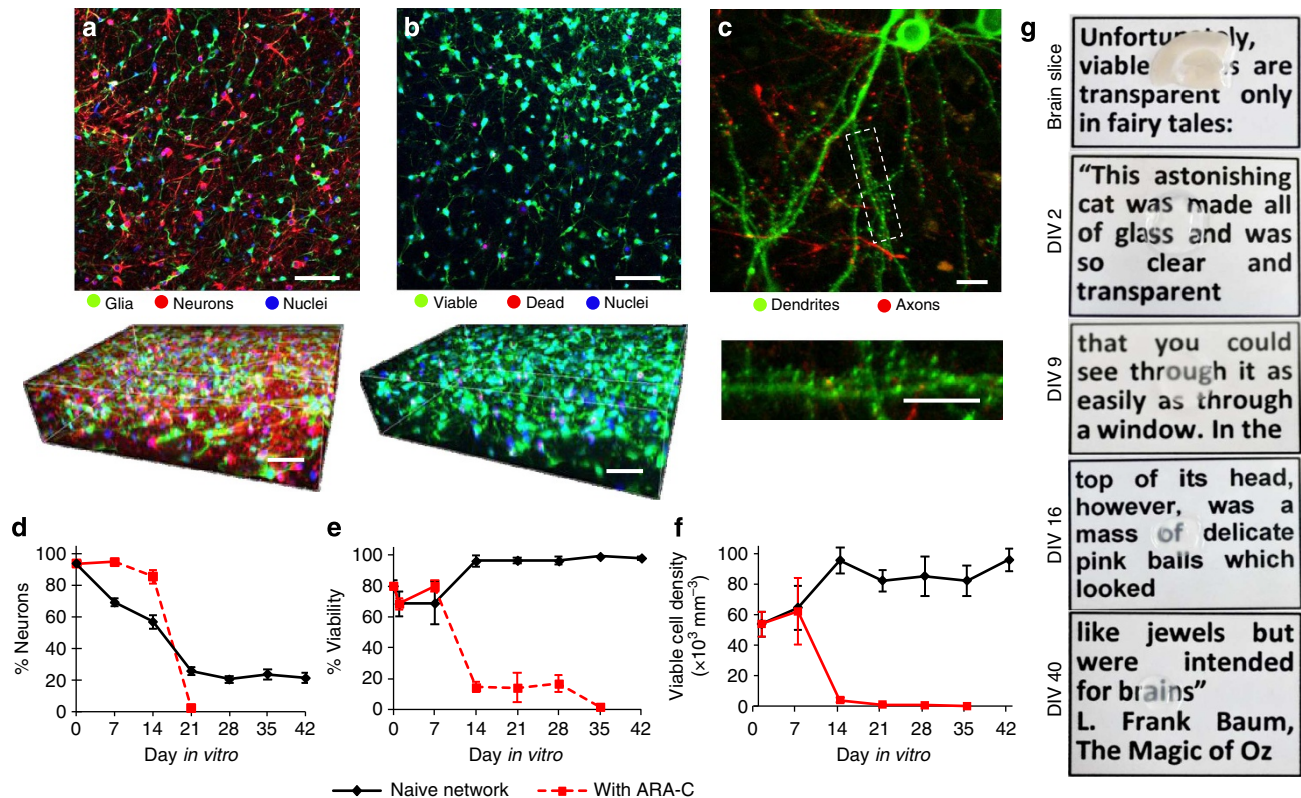


Figure 2 | Development and characteristics of 3D hydrogel-encapsulated dense neural network. Embryonic rat cortical dissociated cells were encapsulated in a Matrigel scaffold and allowed to create a spontaneous network. Images shown and analysed in (a–f) were taken using a confocal microscope. (a) Cellular content immunostains for neurons (red, β III tubulin), glia (green, S100) and nuclei (blue, DAPI), showing confocal sections (a,b,c) and 120- μ m-thick 3D stacks (a,b). (b) Viable (green, calcein) versus dead (red, ethidium homodimer) cells in the network versus total nuclei (blue, DAPI). (c) Synaptic morphology in neurons virally transfected with the synaptic vesicle protein SV2 (red) and the postsynaptic density protein PSD95 (green). Bottom panels: weekly *in vitro* development characteristics of the neuronal cell content (d), viability (e), and network density (f, number of nuclei of viable cells per mm^3) when glial proliferation is normal (black lines) or inhibited using ARA-C (red lines). Broken line indicates disintegrated network, error bars indicate s.e.m. (g) Characteristic scattering by 500- μ m-thick rat cortical brain slice and characteristic optonets photographed over text. Scale bars, 50 μ m (a,b) or 15 μ m (c).

unchanged (Fig. 1e), while allowing the system to reach rates of 200 frames per second for large field-of-view imaging (Fig. 1f, and see Methods for details). Imaged volumes had depths of 150–300 μ m (limited by dye penetration) and in representative networks contained 327, 1,462 and 966 cells (Fig. 3; first network imaged at high magnification, all three networks were imaged at 200 frames per second and 10 volumes per second). Following cell segmentation, the high temporal resolution SLITE movies were converted to dF/F vectors for the entire network (Fig. 3d–f, each row describes the activity of a single active cell over time at 10 samples per second), and calcium transients were detected. Approximately 30% cells in these networks showed functional activity (110/327, 384/1,462 and 346/966, respectively for Fig. 3 networks, Supplementary Movie 7, $29 \pm 13\%$ for the 14 networks): activity traces of the entire network (Fig. 3d–f) as well as of individual cells (Fig. 3g–h, inset in Fig. 3h shows an average calcium transient from a single trace, with best-fit exponential template), showed a high degree of spatiotemporal heterogeneity, not limited to the characteristic burst-dominated activity typically seen in two-dimensional networks using MEAs³². Spontaneous multi-neuronal synchronized activity events were also occasionally observed (Fig. 3f,i, six events detected, Supplementary Movie 8). Different bursts generally did not engage the same cells and their underlying propagation dynamics may nevertheless reflect an underlying spatiotemporal structure (for example, Fig. 3i, Supplementary Movie 9).

Discussion

The advent of cellular- and molecular-level optophysiology tools in recent years has generated much interest in the development of optically-clear or minimally-scattering preparations and tools for providing simplified optical access to large extended functional networks. However, exciting optical clearing approaches like Clarity³³, are currently limited to nonvital applications, whereas large-scale light-sheet imaging³⁴ approaches are limited to lightly-scattering samples where illumination light can be delivered from the side. Our approach provides a functional cellular-resolution interface with large neural populations (containing upwards of 1,000 cells) inside a viable, functional and extended (centimeter-wide) bioengineered neural network. The 3D ECM-like growth environment and conditions were found to support the spontaneous development of morphological and physiological characteristics that are brain-like in terms of cellular and synaptic densities (not shown in earlier *in vitro* studies), neuron:glia ratio (1:4, similar to human cortex³⁵), dependence of viability on glial proliferation (Fig. 2 and Supplementary Fig. 6) and the emergence of spontaneous electrophysiological activity (Fig. 3 and Supplementary Fig. 8). SLITE microscopy was then shown to allow rapid, cellular-resolution dense imaging (without the need for sparse spatial sampling) inside relatively large mm-scale volumes with tight axial sectioning; the use of an amplified femtosecond laser source enables extended line excitation with a good signal-to-noise ratio. Moreover, the new design combining

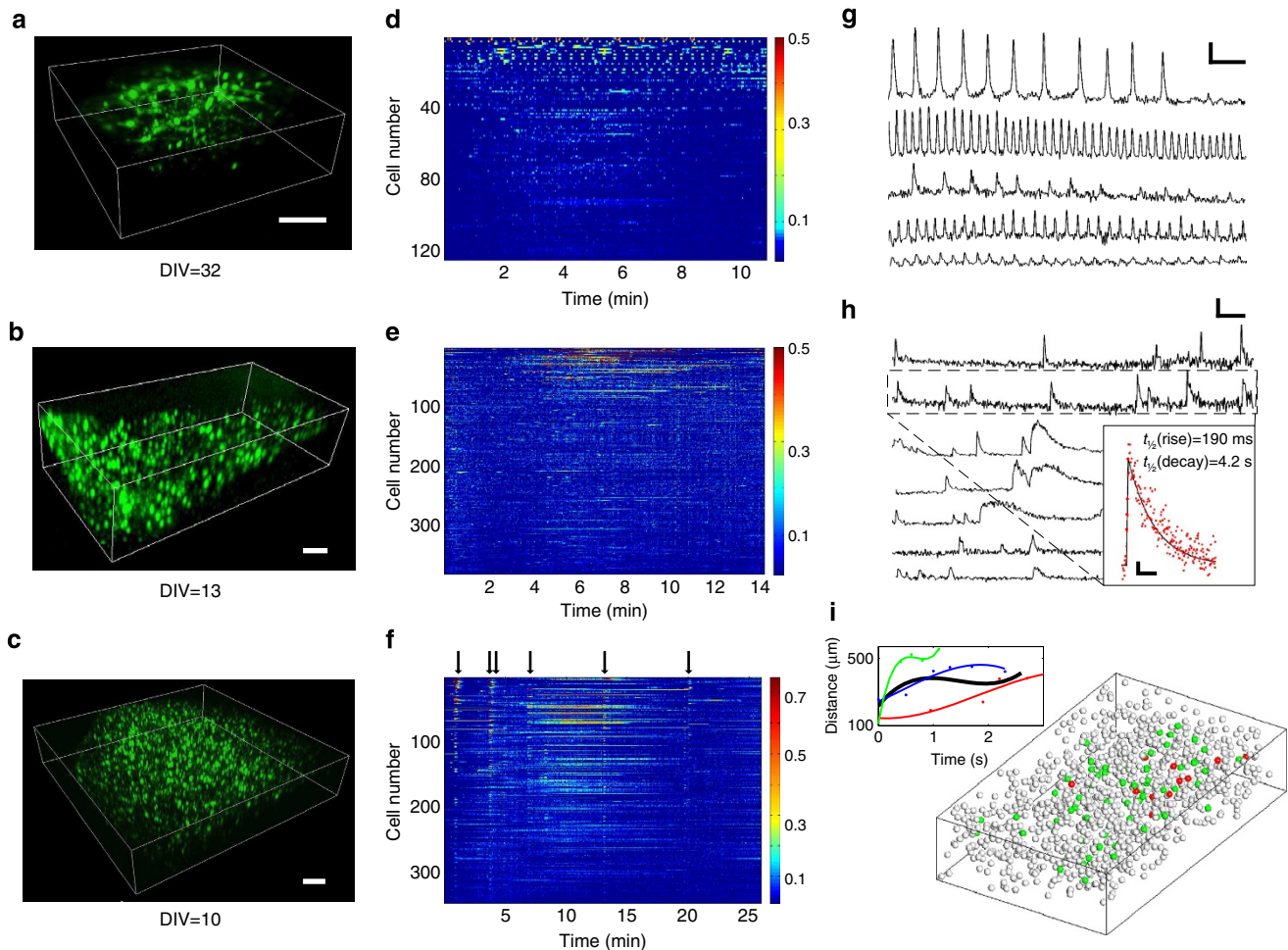


Figure 3 | Networks' functional imaging. (a–c), Volumetric structural images of three networks. Imaged volume dimensions were $200 \times 500 \times 150\ \mu\text{m}^3$ (a, 327 cells) and $600 \times 1,000 \times 200\ \mu\text{m}^3$ (b and c, 1,462 and 966 cells, respectively). Scale bar, $100\ \mu\text{m}$. (d–f) dF/F pseudo-color plots for active cells in each network shown in a–c (121, 384 and 346 cells in d, e and f, respectively). Cells are organized according to their maximal dF/F value. Arrows in f mark network activity bursts. (g–h) dF/F traces of several cells from networks shown in a and b, respectively. Scale bars for g and h are 60 s and dF/F = 0.25, and 60 s and dF/F = 0.5, respectively. Inset in h shows an averaged calcium transient for the marked reference trace (red dots), with best-fit exponential template (solid black line), and rise and decay times to half of the signal maximum (scale bar, 4 s and 0.1 dF/F). (i) Demonstration of a burst spatiotemporal structure in imaged network c is shown. Each sphere represents a cell; red spheres represent cells that fire in the first 1.5 s of the activity (12/50 cells), green spheres represent all the other active cells. Inset shows the time-dependent average distance of all active cells from the burst origin for four different bursts (dots), with fitted trend lines.

TPLSM and SLITE provides both high spatial resolution images and high temporal resolution movies of the same volume, benefitting from the disparate strengths of each modality in a single imaging session (Supplementary Movie 8 and Supplementary Fig. 9). Unlike other state-of-the-art multiphoton imaging systems^{15–17}, SLITE microscopy does not rely on rapid serial point-scanning (see Supplementary Table 1 for comparison), and thus fundamentally moves the imaging bottleneck from planning and optimizing complex scan trajectories to the performance limits of the detection camera collecting the light emitted from the illuminated focal plane (200 frames per second in our experiments). When combined with contemporary camera systems operating at multi-kHz frame rates it is well poised for tackling the challenges of ultra rapid multiphoton imaging in a large network, which is required for millisecond-accurate imaging using calcium¹⁷ or even voltage³⁶ indicators. Dense spatial sampling has additional advantages in the context of neural imaging, enabling simpler correction of movement artifacts than hopping systems, and the ability to monitor activity in developing, highly-motile networks. Although

presented here in the context of imaging a bioengineered neural tissue, SLITE and related rapid TF methods^{21,37} can clearly also be used to image neuronal activity in other lightly-scattering preparations such as *c-elegans*³⁷ and zebrafish. Technical adaptations could potentially also have an important role in imaging cortical network activity patterns *in vivo* and may find additional applications in other fields of biomedicine where relatively rapid dense volumetric imaging is advantageous, including moving tissues such as the heart, and super-resolution imaging, where rapid planar acquisition may significantly enhance imaging rate³⁸.

Further development and refinement of this new type of *in vitro* neural interfacing technology using, for example, the wide variety of optogenetic probes for monitoring^{13,39} and/or controlling⁴⁰ neuronal activity using complementary photostimulation systems^{41,42}, could lead to a new generation of optically accessible and sensitive bioengineered networks or 'optonets', where even 3D growth and connectivity could potentially be optically guided^{43,44}. Such an optical-neuronal interface may find applications in the *in vitro* study of neuronal

computations, testing of pharmacological agents and their effects on network activity patterns, and could potentially also lead to a new generation of bio-hybrid medical devices and applications.

Methods

Optical system design. The dual SLITE-TPLSM system was designed for rapid functional imaging of a large field of view with single cell resolution, and is based on the development of a single-optical-axis TF setup, to enable easy combination of a TF microscope with TPLSM or other optical modalities.

A regeneratively amplified laser source (RegA 9000, pumped and seeded by a Vitesse duo; Coherent) provides 800 nm, 200 fs pulses with up to 1.5 μJ per pulse (measured at the sample plane) at 150 KHz repetition rate. Illumination power is controlled by a Pockels cell (Conoptics), and a beam expander is used to expand the laser beam cross section. For SLITE microscopy, the beam is scanned in the line lateral direction using a single scanning mirror (Cambridge Technologies), focused by a cylindrical lens ($f = 100$ mm) on a transmission grating surface, and diffracted by the DPG (Wasatch Photonics). The prism angles ($48^\circ \times 42^\circ \times 90^\circ$, BK7 glass) and the diffraction grating groove density (1,200 lines mm^{-1}) are designed to refract and diffract the laser's central wavelength (800 nm) toward the same direction of the incoming light propagation, and have an efficiency of 85% for both polarization states. The microscope's tube (Nikon) and objective lenses (Zeiss $\times 10$ NA = 0.45, Olympus $\times 20$ NA = 0.5; actual magnifications = 12 and 22, respectively due to the different tube), mounted in a 4f configuration, image the grating surface onto the objective focal plane—where a temporally focused line is obtained. We image this line using an epi-detection scheme (Fig. 1a), where the fluorescence light is reflected by a dichroic mirror (Chroma) towards an EMCCD camera (iXon 885, Andor Technology). Each line scan cycle is synchronized with one image acquisition (Supplementary Fig. 2). The camera's maximal imaging rate is 200 frames s^{-1} for 100 lines per image reading, and therefore we also used 5 ms for the line scanning. The objective lens was moved axially by a piezoelectric device (Nanomotum) with rates of up to 20 Hz and controlled amplitude of up to several millimetres, with resolution of 50 nm. After picking an axial scanning amplitude and rate, the planar images number per cycle (usually 10–20 images per 100 ms, and axial range of 150–300 μm in our experiments) defines the axial resolution. To minimize the tissue exposure to light, the Pockels cell blocked the laser beam intensity when the piezoelectric device returned the objective lens to its initial position at the end of volumetric scanning cycle (Supplementary Fig. 2); thus only 90% of the images contained information.

Switching from SLITE microscopy to TPLSM is simply done by replacing the cylindrical lens and DPG with a scan lens (Fig. 1a), two galvanometric mirrors are used to scan the beam, and the dichroic mirror is rotated to direct the fluorescence signal toward a photomultiplier tube (Hamamatsu). TPLSM images were acquired using the ScanImage software⁴⁵, typically with 512×512 pixels and a 4 ms per line rate. Therefore, a single planar image acquisition time was 400 times longer than SLITE image.

Preparation of 3D neural cultures. The animal experiments and procedures were approved by the Institutional Animal Care Committee at Technion—Israel Institute of Technology and were in accord with the National Institutes of Health Guide for the Care and Use of Laboratory Animals.

We removed and diced cortical tissue from embryonic day 18 (E18) Sprague Dawley rats in cold phosphate-buffered saline (PBS) solution with 20 mM glucose, mechanically dissociated neural cells (by forcing a few times through a pipette), and filtered the suspension using a 70 μm cell strainer (Biologix). A total of 1.2–1.8 million cells were encapsulated in 30 μl Matrigel scaffold (Growth factor reduced, BD Biosciences). Culturing media was composed of Minimal Essential Media (MEM, Sigma) containing 17 mM glucose, 100 $\mu\text{l ml}^{-1}$ of NU Serum (BD Biosciences), 30 mg ml^{-1} of L-glutamine (Sigma), 1:500 B-27 supplement (Gibco), 50 ng ml^{-1} of nerve growth factor (NGF, Alomone labs), 10 ng ml^{-1} of brain-derived neurotrophic factor (BDNF, R&D systems), 25 $\mu\text{g ml}^{-1}$ of insulin (Sigma), and 2 $\mu\text{g ml}^{-1}$ of gentamicin. Half the volume of the culturing media was replaced twice a week. In a second group of cultures, 3 μM of arabinofuranosyl cytidine (ARA-C, Sigma) to inhibit glial cell proliferation was added once at DIV3.

Staining and image analysis. For whole-gel viability staining, a MEM solution containing 0.4 μM of ethidium homodimer (Sigma), a nucleic acid fluorescent tag designed to stain dead cells red, 8 μM calcein (Sigma), which stains live cells green and 6 nM of 4',6 diamidino-2-phenylindole (DAPI, Sigma), a fluorescent tag that stains the nuclei of all cells blue was added. Cultures were incubated for 2.5 h at 37 $^\circ\text{C}$ while shaking, and then washed. Imaging was performed using a confocal microscope (Zeiss, LSM 700). Imaris software (Bitplane) was used for counting the total number of cells visible in one plane. The counts of the live and dead cells, and total nuclei in each image were used to calculate the vitality percentage for each sample: each week *in vitro* $n = 6$ –10 naive networks (3–5 cell extractions $\times 2$ replicates each) and $n = 2$ –8 ARA-C treated cultures (1–4 cell extractions $\times 2$ replicates each) were evaluated. Viable cell density was evaluated by counting nuclei in confocal image stacks of $320 \times 320 \times 50$ μm ($n = 3$ –8 naive and $n = 2$ –8 ARA-C treated networks for each week), and multiplying by the corresponding

viability rate. For whole-gel differential immunostaining, cultures were fixed for 2 h using a 4% paraformaldehyde solution in PBS, followed by 4 h of permeabilization and a blocking process in 0.3–1% Triton and 4% fetal bovine serum solution in PBS. The cultures were washed, and the primary antibodies Mouse-Anti Beta III Tubulin (1:400, Promega), a marker of neuronal cells, and Rabbit-Anti S100 (1:200, Sigma), a marker of glial cells, were added, and incubated overnight at 4 $^\circ\text{C}$. Cultures were washed and secondary antibodies, CY 3 Conjugated Goat-Anti-Mouse Immunoglobulin (1:100, Jackson) and Dylight 488 Conjugated Goat-Anti-Rabbit IgG (1:100, Jackson), were added along with DAPI (6 nM, Sigma), designed to stain the nuclei of all cells and incubated for at least 4 h or overnight and washed. The different cell types were counted using ImageJ cell counter; $n = 6$ –14 naive networks (3–7 cell extractions $\times 2$ replicates each) and $n = 4$ ARA-C treated cultures (two cell extractions $\times 2$ replicates each) were evaluated.

For activity imaging, cultures were incubated for 2–2.5 h at 37 $^\circ\text{C}$ with the organic calcium indicator Fluo-4 (2–3 $\mu\text{l ml}^{-1}$ of a 1 $\mu\text{g l}^{-1}$ solution, Invitrogen). SLITE raw data consisted of planar images at different depths and time points. Images were grouped according to their axial position and cell segmentation for each plane was performed using CellProfiler (cells with centre position in adjacent planes were merged) or Imaris. Fluorescence signals were normalized according to $\frac{\Delta F}{F}(t) = \frac{F(t) - F_0}{F_0}$, where F_0 is each cell's average signal during the experiment's first 30 s (after removing dark current), and $F(t)$ is its temporal fluorescence signal. The identification of calcium transients was performed semi-automatically: a peak detection software (Peakdet Matlab function) performed initial analysis and a user manually added or cancelled detected peaks.

Structural imaging of network development. Cell cultures were transfected at DIV2 with lentiviral vectors encoding for Cerulean:SV2 (ref. 46) and PSD95:EGFP³². Time-lapse imaging were performed at 37 $^\circ\text{C}$ and controlled CO₂ conditions (protocol given in ref. 32) at DIV17–30 for 3–5 days using a custom-built Confocal Laser Scanning Microscope based on a Zeiss AxioObserver.Z1 using a 40 $\times 1.3$ NA Fluor objective. Cultures were imaged every 30 or 60 min by averaging 4–6 images collected at each of 10 focal planes spaced 0.8 μm apart.

References

- Potter, S. M. Distributed processing in cultured neuronal networks. *Prog. Brain Res.* **130**, 49–62 (2001).
- Dichter, M. A. Rat cortical neurons in cell culture: culture methods, cell morphology, electrophysiology, and synapse formation. *Brain Res.* **149**, 279 (1978).
- Shahaf, G. & Marom, S. Learning in networks of cortical neurons. *J. Neurosci.* **21**, 8782–8788 (2001).
- Marom, S. & Shahaf, G. Development, learning and memory in large random networks of cortical neurons: lessons beyond anatomy. *Q. Rev. Biophys.* **35**, 63–87 (2002).
- Stett, A. et al. Biological application of microelectrode arrays in drug discovery and basic research. *Anal. Bioanal. Chem.* **377**, 486–495 (2003).
- Bishop, H. I. & Zito, K. The downs and ups of sensory deprivation: evidence for firing rate homeostasis *in vivo*. *Neuron* **80**, 247–249 (2013).
- Franze, K. & Guck, J. The biophysics of neuronal growth. *Rep. Prog. Phys.* **73**, 094601 (2010).
- Edelman, D. B. & Keefer, E. W. A cultural renaissance: *in vitro* cell biology embraces three-dimensional context. *Exp. Neurol.* **192**, 1–6 (2005).
- Pautot, S., Wyart, C. & Isacoff, E. Y. Colloid-guided assembly of oriented 3D neuronal networks. *Nat. Methods* **5**, 735–740 (2008).
- Irons, H. R. et al. Three-dimensional neural constructs: a novel platform for neurophysiological investigation. *J. Neural Eng.* **5**, 333–341 (2008).
- Heuschkel, M., Wirth, C., Steidl, E.-M. & Buisson, B. In *Advances in Network Electrophysiology* (eds Taketani, Makoto. & Baudry, Michel.) 69–111 (Springer, 2006).
- Musick, K., Khatami, D. & Wheeler, B. C. Three-dimensional micro-electrode array for recording dissociated neuronal cultures. *Lab Chip* **9**, 2036–2042 (2009).
- Chen, T.-W. et al. Ultrasensitive fluorescent proteins for imaging neuronal activity. *Nature* **499**, 295–300 (2013).
- Cheng, A., Goncalves, J. T., Golshani, P., Arisaka, K. & Portera-Cailliau, C. Simultaneous two-photon calcium imaging at different depths with spatiotemporal multiplexing. *Nat. Methods* **8**, 139–142 (2011).
- Gobel, W., Kampa, B. M. & Helmchen, F. Imaging cellular network dynamics in three dimensions using fast 3D laser scanning. *Nat. Methods* **4**, 73–79 (2007).
- Katona, G. et al. Fast two-photon *in vivo* imaging with three-dimensional random-access scanning in large tissue volumes. *Nat. Methods* **9**, 201–208 (2012).
- Grewe, B. F., Langer, D., Kasper, H., Kampa, B. M. & Helmchen, F. High-speed *in vivo* calcium imaging reveals neuronal network activity with near-millisecond precision. *Nat. Methods* **7**, 399–405 (2010).

18. Kerr, J. N. D., Greenberg, D. & Helmchen, F. Imaging input and output of neocortical networks *in vivo*. *Proc. Natl Acad. Sci. USA* **102**, 14063–14068 (2005).
19. Oron, D., Tal, E. & Silberberg, Y. Scanningless depth-resolved microscopy. *Opt. Express* **13**, 1468–1476 (2005).
20. Dana, H. & Shoham, S. Numerical evaluation of temporal focusing characteristics in transparent and scattering media. *Opt. Express* **19**, 4937–4948 (2011).
21. Cheng, L. C. *et al.* Spatiotemporal focusing-based widefield multiphoton microscopy for fast optical sectioning. *Opt. Express* **20**, 8939–8948 (2012).
22. Tal, E., Oron, D. & Silberberg, Y. Improved depth resolution in video-rate line-scanning multiphoton microscopy using temporal focusing. *Opt. Lett.* **30**, 1686–1688 (2005).
23. Zhu, G., van Howe, J., Durst, M., Zipfel, W. & Xu, C. Simultaneous spatial and temporal focusing of femtosecond pulses. *Opt. Express* **13**, 2153–2159 (2005).
24. Durst, M., Zhu, G. & Xu, C. Simultaneous spatial and temporal focusing for axial scanning. *Opt. Express* **14**, 12243–12254 (2006).
25. Papagiakoumou, E., de Sars, V., Oron, D. & Emiliani, V. Patterned two-photon illumination by spatiotemporal shaping of ultrashort pulses. *Opt. Express* **16**, 22039–22047 (2008).
26. Papagiakoumou, E. *et al.* Scanless two-photon excitation of channelrhodopsin-2. *Nat. Methods* **7**, 848–854 (2010).
27. Therrien, O., Aubé, B., Pagès, S., Koninck, P. D. & Côté, D. Wide-field multiphoton imaging of cellular dynamics in thick tissue by temporal focusing and patterned illumination. *Biomed. Opt. Express* **2**, 696–704 (2011).
28. Dana, H., Kruger, N., Ellman, A. & Shoham, S. Line temporal focusing characteristics in transparent and scattering media. *Opt. Express* **21**, 5677–5687 (2013).
29. Dana, H. & Shoham, S. Remotely scanned multiphoton temporal focusing by axial grism scanning. *Opt. Lett.* **37**, 2913–2915 (2012).
30. Mostany, R. *et al.* Altered Synaptic Dynamics during Normal Brain Aging. *J. Neurosci.* **33**, 4094–4104 (2013).
31. Theer, P. & Denk, W. On the fundamental imaging-depth limit in two-photon microscopy. *J. Opt. Soc. Am. A Opt. Image Sci. Vis.* **23**, 3139–3149 (2006).
32. Minerbi, A. *et al.* Long-term relationships between synaptic tenacity, synaptic remodeling, and network activity. *PLoS Biol.* **7**, e1000136 (2009).
33. Chung, K. *et al.* Structural and molecular interrogation of intact biological systems. *Nature* **332**–337 (2013).
34. Ahrens, M. B., Orger, M. B., Robson, D. N., Li, J. M. & Keller, P. J. Whole-brain functional imaging at cellular resolution using light-sheet microscopy. *Nat. Methods* **10**, 413–420 (2013).
35. Nedergaard, M., Ransom, B. & Goldman, S. A. New roles for astrocytes: redefining the functional architecture of the brain. *Trends Neurosci.* **26**, 523–530 (2003).
36. Kralj, J. M., Douglass, A. D., Hochbaum, D. R., Maclaurin, D. & Cohen, A. E. Optical recording of action potentials in mammalian neurons using a microbial rhodopsin. *Nat. Methods* **9**, 90–95 (2011).
37. Schrödel, T., Prevedel, R., Aumayr, K., Zimmer, M. & Vaziri, A. Brain-wide 3D imaging of neuronal activity in *Caenorhabditis elegans* with sculpted light. *Nat. Methods* **10**, 1013–1020 (2013).
38. Vaziri, A., Tang, J., Shroff, H. & Shank, C. Multilayer three-dimensional super resolution imaging of thick biological samples. *Proc. Natl Acad. Sci. USA* **105**, 20221–20226 (2008).
39. Tian, L. *et al.* Imaging neural activity in worms, flies and mice with improved GCaMP calcium indicators. *Nat. Methods* **6**, 875–881 (2009).
40. Boyden, E. S., Zhang, F., Bamberg, E., Nagel, G. & Deisseroth, K. Millisecond-timescale, genetically targeted optical control of neural activity. *Nat. Neurosci.* **8**, 1263–1268 (2005).
41. Andrasfalvy, B., Zemelman, B., Tang, J. & Vaziri, A. Two-photon single-cell optogenetic control of neuronal activity by sculpted light. *Proc. Natl. Acad. Sci. USA* **107**, 11981–11986 (2010).
42. Reutsky-Gefen, I. *et al.* Holographic optogenetic stimulation of patterned neuronal activity for vision restoration. *Nat. Commun.* **4**, 1509 (2013).
43. Sarig-Nadir, O., Livnat, N., Zajdman, R., Shoham, S. & Seliktar, D. Laser photoablation of guidance microchannels into hydrogels directs cell growth in three dimensions. *Biophys. J.* **96**, 4743–4752 (2009).
44. Wylie, R. G. *et al.* Spatially controlled simultaneous patterning of multiple growth factors in three-dimensional hydrogels. *Nat. Mater.* **10**, 799–806 (2011).
45. Pologruito, T. A., Sabatini, B. L. & Svoboda, K. ScanImage: flexible software for operating laser scanning microscopes. *Biomed. Eng. Online* **2**, 13 (2003).
46. Fisher-Lavie, A., Zeidan, A., Stern, M., Garner, C. C. & Ziv, N. E. Use dependence of presynaptic tenacity. *J. Neurosci.* **31**, 16770–16780 (2011).

Acknowledgements

We gratefully acknowledge the financial support of the European Research Council (grant #211055), and of the Technion's Russel Berrie Nanotechnology Institute. We thank the Lorey I. Lokey LS&E infrastructure unit, Erez Shor, Tony Yensinger, Avigdor Meir, Shem-Tov Halevi and Wasatch Photonics for technical assistance, and Shimon Marom, Noam Ziv, Dvir Yelin, Moti Segev, Itamar Kahn, Sanjeev K. Mahto, Adi Schejter, Nairouz Farah and Steve Krupa for their support, many helpful discussions and comments on the manuscript. We thank the HHMI JFRC GENIE project for generously authorizing the use of GCaMP6 (Supplementary figure 8).

Author contributions

H.D., A.M. and S.S. designed the study. H.D. developed, characterized and optimized the optical system, and A.M. developed the 3D network growth protocol, chamber and all characterizations, with assistance from I.B. SLITE Imaging experiments and their analysis were performed by H.D., S.P. and A.M. Synaptic transfection and time-lapse imaging was performed by R.D. S.S. supervised the project and prepared the manuscript together with all co-authors.

Additional information

Supplementary Information accompanies this paper on <http://www.nature.com/naturecommunications>

Competing financial interests: Shy Shoham, Hod Dana and Anat Marom are named inventors on Technion patent applications related to methods described in the manuscript (US/13/733,163 and PCT/IB2012/056464).

Reprints and permission information is available online at <http://npg.nature.com/reprintsandpermissions/>

How to cite this article: Dana, H. *et al.* Hybrid multiphoton volumetric functional imaging of large-scale bioengineered neuronal networks. *Nat. Commun.* **3**:3997 doi: 10.1038/ncomms4997 (2014).